## Research

Check for updates

**Author for correspondence:**
Mason A. Porter
e-mail: mason@math.ucla.edu

# Quasiperiodic granular chains and Hofstadter butterflies

Alejandro J. Martínez[1,2], Mason A. Porter[3] and P. G. Kevrekidis[4]

[1]Oxford Centre for Industrial and Applied Mathematics, Mathematical Institute, University of Oxford, Oxford OX2 6GG, UK
[2]Computational Biology Laboratory, Fundación Ciencia & Vida, Avda. Zañartu 1482, Ñuñoa, Santiago, Chile
[3]Department of Mathematics, University of California, Los Angeles, CA 90095, USA
[4]Department of Mathematics and Statistics, University of Massachusetts, Amherst, MA 01003, USA

MAP, 0000-0002-5166-0717

We study quasiperiodicity-induced localization of waves in strongly precompressed granular chains. We propose three different set-ups, inspired by the Aubry–André (AA) model, of quasiperiodic chains; and we use these models to compare the effects of on-site and off-site quasiperiodicity in nonlinear lattices. When there is purely on-site quasiperiodicity, which we implement in two different ways, we show for a chain of spherical particles that there is a localization transition (as in the original AA model). However, we observe no localization transition in a chain of cylindrical particles in which we incorporate quasiperiodicity in the distribution of contact angles between adjacent cylinders by making the angle periodicity incommensurate with that of the chain. For each of our three models, we compute the Hofstadter spectrum and the associated Minkowski–Bouligand fractal dimension, and we demonstrate that the fractal dimension decreases as one approaches the localization transition (when it exists). We also show, using the chain of cylinders as an example, how to recover the Hofstadter spectrum from the system dynamics. Finally, in a suite of numerical computations, we demonstrate localization and also that there exist regimes of ballistic, superdiffusive, diffusive and subdiffusive transport. Our models provide a flexible

## THE ROYAL SOCIETY
PUBLISHING

set of systems to study quasiperiodicity-induced analogues of Anderson phenomena in granular chains that one can tune controllably from weakly to strongly nonlinear regimes.

This article is part of the theme issue 'Nonlinear energy transfer in dynamical and acoustical systems'.

## 1. Introduction

Quasicrystals are solids whose structure is ordered but not periodic [1]. For many years, it was thought that quasicrystals could only be produced artificially. However, almost a decade ago, the first natural quasicrystal was found in Russia [2]. A common type of quasicrystal arises when atoms are arranged so that they possess symmetries, such as 5-fold symmetry, that are forbidden to periodic crystals.[1] A famous two-dimensional (2D) example is a Penrose tiling [4]. More generally, quasiperiodic structures can exist in any number of dimensions as structures with a broken translational symmetry. In one dimension (1D), the most common models used in the study of quasiperiodic systems are a Fibonacci quasicrystal [5] and the Aubry–André (AA) model [6]. These models are topologically equivalent to each other [7], in the sense that it is possible to continuously deform one into the other without closing any gaps in the bulk spectrum.

A key feature of quasiperiodic potentials, arising prominently in the study of Schrödinger equations [6], is the transition from a 'metallic' phase (in which all eigenstates are delocalized) to an 'insulating' phase (in which they are localized). See, for example, the analysis in [8,9] and the experiments in [10]. It is of considerable interest to extend these studies in various ways, including to nonlinear systems (see e.g. the work of [11] and references therein), many-body systems, discrete systems and settings with controllable interactions. There have been relevant investigations in both bosonic and fermionic settings [12,13], as well as recent experimental [14] and theoretical [15] investigations of localization–delocalization transitions in driven AA models. Other recent work has explored disorder-free localization transitions in both one dimension and higher dimensions [16,17].

In this paper, we study the effects of quasiperiodicity in strongly precompressed granular chains [18,19], in which neighbouring particles interact with each other according to a Hertzian potential. Our aim is to illustrate that localization of eigenmodes can occur in quasiperiodic granular chains and to explore the conditions—with respect to both models and experimental set-ups—in which it occurs. We illuminate these conditions by comparing a variety of different models with one or both of on-site and off-site quasiperiodic structures. As demonstrated in a wealth of research over more than three decades [20], granular chains are extremely versatile, as one can: adjust interaction potentials; readily tune them between almost linear, weakly nonlinear and strongly nonlinear regimes by applying different precompression strengths; construct them using particles of different sizes, shapes and material properties; and so on. This has yielded a wealth of insights about a diverse variety of physical phenomena, including acoustic realizations of many concepts from condensed-matter physics [21]. Most centrally for our discussion, this includes the dynamics of wave transport and localization in disordered nonlinear systems in both theoretical [22,23] and experimental [24] studies. Other phenomena (both theoretical and applied) from condensed-matter and quantum physics that have been realized in granular crystals include an analogue of a Ramsauer–Townsend resonance in the form of a square well [25], switching and rectification [26] and others. More broadly, granular chains provide a wonderful playground that enables systematic exploration of the role of lattice structure (e.g. material heterogeneity [27,28]) and fundamental dynamic (e.g. rogue waves [29]) and thermodynamic (e.g. equipartition [30]) phenomena.

The remainder of our paper is organized as follows. In §2, we briefly review the AA model. In §3, we present three models of 1D quasiperiodic lattices: two with on-site quasiperiodicity

[1]By the so-called 'crystallographic restriction', crystals can have only certain rotational symmetries: 2-fold, 3-fold, 4-fold or 6-fold symmetry [3].

**3**

rsta.royalsocietypublishing.org *Phil. Trans. R. Soc. A* **376**: 20170139

and one with off-site quasiperiodicity. In §4, we linearize the governing equations of our three models. In §5, we demonstrate that such models can possess a Hofstadter butterfly structure, and we propose a method to recover such structure from the dynamics. In §6, we examine energy transport and localization in our models. We conclude and suggest some interesting directions for future research in §7.

## 2. A brief review of the Aubry–André model

The prototypical form of the AA model at the level of a tight-binding model is

$$E\Psi_n = \Psi_{n+1} + \Psi_{n-1} + \lambda V(nq + r)\Psi_n, \tag{2.1}$$

where $\Psi$ is a wave function, $n$ indexes the lattice site, $E$ denotes the energy, $V$ is a potential and $\lambda$ is a parameter. We suppose that the on-site energy is modulated by a lattice distortion with wave vector $q \in \mathbb{R}$, which is incommensurate with $2\pi$ and is offset by a phase $r$. We also suppose that $V(x) = V(x + 2\pi n)$, where $x \in \mathbb{R}$ and $n \in \mathbb{Z}$.

In [6], Aubry and André proved several fundamental properties of the eigenmodes of (2.1). They showed that a ground state exists and, when $q$ is not a Liouville number, that it undergoes a transition from analyticity for $\lambda < \lambda_c$ to non-analyticity for $\lambda > \lambda_c$ for some critical value $\lambda_c(q)$. That is, $q \in \mathbb{R} \setminus \mathbb{Q}$ and there exist $\gamma$ and $r$ such that

$$\left| \frac{q}{2\pi} - \frac{p_1}{p_2} \right| > \gamma \frac{1}{p_2^r} \tag{2.2}$$

is satisfied for any rational number $p_1/p_2$.

Aubry and André also showed, using a perturbative approach, that the analyticity breaking leads to very rich spatial properties of the eigenmodes of (2.1). One can write the eigenmodes of the modulated system as

$$\Psi_n(k) = e^{ikn} + \lambda \sum_{m=-\infty}^{\infty} \frac{v_m \, e^{im(qn+h)}}{2[\cos(mq+k) - \cos(k)]}, \tag{2.3}$$

where $v_m$ are the coefficients of the Fourier expansion of $V$. The eigenmodes and eigenvalues for $\lambda = 0$ are given by $e^{ikn}$ and $2\cos(k)$, respectively. For the series in (2.3) to be convergent, one needs to satisfy a Diophantine condition. That is, there exist two positive constants $K$ and $\beta$ such that

$$\left| \frac{k}{\pi} + m\frac{q}{2\pi} - n \right| > \frac{K}{m^{1+\beta}} \tag{2.4}$$

for any integers $m$ and $n$.

For simplicity, consider the special case in which the phase $r = 0$ and the potential $V = \cos(2\pi\xi n)$, where $\xi = (1 + \sqrt{5})/2$ is the golden ratio. Equation (2.1) then takes the following form:

$$E\Psi_n = \Psi_{n+1} + \Psi_{n-1} + \lambda \cos(2\pi\xi n)\Psi_n. \tag{2.5}$$

In this case, Aubry and André showed for $\lambda > \bar{\lambda}_c = 2$ that all of the eigenmodes of (2.1) are exponentially localized, as in the Anderson model (in which the potential $V$ is disordered rather than quasiperiodic) [31], with the same characteristic localization length

$$\zeta = \frac{1}{\ln(\lambda/2)}. \tag{2.6}$$

That is, $\Psi_n$ decays asymptotically as $e^{-n/\zeta}$ as $n \to \infty$. However, when $\lambda < \bar{\lambda}_c = 2$, most eigenmodes consist of extended, modulated plane waves. Interestingly, this implies that the loss of analyticity is also associated with a transition at $\bar{\lambda}_c$ to spatial localization of the eigenmodes. This transition is called a *localization transition* or *Aubry–André transition*. This result is a generic phenomenon in Schrödinger lattices, and it is thus relevant for a diverse variety of physical systems [10,32–34], including photonic lattices, Bose–Einstein condensates and many others. Additionally, the spectra

of the corresponding Schrödinger operators (with two or even more frequencies) is a topic of intense mathematical interest; see e.g. [35] and references therein.

## 3. Implementing the Aubry–André model in granular chains

Several recent studies have generalized conventional granular chains in various ways. They have yielded several interesting insights, and they promise to result in a host of others in the coming years [20,21]. One type of a generalized granular chain is a *cradle system* [36], in which particles are attached to linear oscillators, enabling the use of on-site potentials in a way that is independent of particle–particle interactions. Several potential realizations of such a setting were given in [37] (although, to the best of our knowledge, they have yet to be implemented experimentally). Another fascinating variant arises from examining a chain of particles with internal resonators, such as by coupling a secondary particle inside a principal one. This leads to a locally resonant granular chain, which is sometimes called a *mass-in-mass* (or *mass-with-mass*, if the secondary particle is external) chain [38–40]. Additionally, the use of particles with non-spherical geometries can drastically modify particle–particle interactions. For instance, with cylindrical particles (which are arranged so that their sides are in contact), although one has the same functional relation between the force and the displacements as with spherical particles, one can tune the magnitude of such interactions by changing the contact angle between adjacent cylinders [41,42].

We will consider granular chains with all of the above types of variations. The equations of motion in our general setting are

$$\ddot{u}_n = \underbrace{\alpha_n[\delta_n + u_{n-1} - u_n]_+^{3/2} - \alpha_{n+1}[\delta_{n+1} + u_n - u_{n+1}]_+^{3/2}}_{\text{Hertzian interaction}}$$

$$- \underbrace{\beta_n u_n}_{\text{elastic restitution}} - \underbrace{\gamma_n(u_n - v_n)}_{\text{mass-in-mass interaction}}, \tag{3.1}$$

$$\ddot{v}_n = \gamma_n(u_n - v_n), \tag{3.2}$$

where $u_n$ is the displacement of the $n$th particle (where $n \in \{1, 2, \ldots, N\}$) measured from its equilibrium position in the initially compressed chain, $v_n$ is the displacement of the $n$th interior mass (when one particle is located inside another), and

$$\delta_n = \left(\frac{F_0}{A_n}\right)^{2/3} \tag{3.3}$$

is a static displacement for each particle that arises from the static load $F_0 = \text{const}$. There is a Hertzian interaction between a pair of particles only when they are in contact, so each particle is affected directly only by its nearest neighbours and experiences a force from a neighbour only when it overlaps with it. This yields

$$[x]_+ = \begin{cases} x, & \text{if } x > 0, \\ 0, & \text{if } x \leq 0. \end{cases} \tag{3.4}$$

In our subsequent discussions (see §3), we will consider various special cases of (3.1,3.2), depending on the type of particle that we use to construct the chains. Specifically, we work with three different models: two of them have spherical particles, and one has cylindrical particles. For our analysis and computations, we assume that the prefactors $\alpha_n$, $\beta_n$ and $\gamma_n$ vary sinusoidally in space according to the following formulae:

$$\alpha_n = \bar{\alpha}_1 + \bar{\alpha}_2 \cos(2\pi n \xi), \tag{3.5}$$

$$\beta_n = \bar{\beta}[1 + \cos(2\pi n \xi)], \tag{3.6}$$

$$\gamma_n = \bar{\gamma}[1 + \cos(2\pi n \xi)], \tag{3.7}$$

where $\xi$ is the golden mean $(\sqrt{5}+1)/2$ (unless we explicitly state otherwise), $\bar{\alpha}_1 > \bar{\alpha}_2 \geq 0$ and $\bar{\beta}$, $\bar{\gamma} \geq 0$. For simplicity, we separately examine the effects of (3.5)–(3.7). This leads to three different models in which it may be possible to observe an AA transition. In equations (3.5)–(3.7), the quasiperiodicity parameters $\bar{\alpha}_2$, $\bar{\beta}$ and $\bar{\gamma}$ determine the strengths of the modulations for the different terms in equations (3.1,3.2).

## (a) On-site quasiperiodicity: two different variants of the Aubry–André model using spherical particles

In this subsection, we discuss the effect of an on-site quasiperiodicity on the dynamics of a granular chain by considering chains of spherical particles with local potentials. We set $\bar{\alpha}_2 = 0$ in equation (3.5), so the coupling parameter $\alpha_n$ is given by $\alpha_n = A_n/m_n$, where

$$A_n = \frac{4E_{n-1}E_n \left( \frac{R_{n-1}R_n}{R_{n-1}+R_n} \right)^{1/2}}{3[E_n(1 - v_{n-1}^2) + E_{n-1}(1 - v_n^2)]} \tag{3.8}$$

and the $n$th particle has elastic modulus $E_n$, Poisson ratio $v_n$, radius $R_n$ and mass $m_n$. We assume that the particles are identical, so $E_n = E$, $v_n = v$, $R_n = R$ and $m_n = m$. This, in turn, implies that $\alpha_n = \bar{\alpha}_1$, and we let $\bar{\alpha}_1 = 1$ without loss of generality.

### (i) Model Ia: $\bar{\beta} \neq 0$ and $\bar{\alpha}_2 = \bar{\gamma} = 0$

Suppose that the particles in the chain are attached to a mechanical restitution mechanism, such that there is a linear force in the equations of motion (3.1,3.2). This can describe a Newton's cradle, a system in which particles are aligned in one dimension and are suspended from a ceiling by strings so that the particles collide with each other along one dimension and oscillate. In figure 1a, we show a schematic of this system. Studies of this system have focused primarily on waves that arise by releasing one of the particles at one end with some speed [37]. This produces a transfer of energy across the chain in the form of travelling waves [36]. Mulansky and Pikovsky studied disorder in closely related (nonlinearly coupled, and locally linear or nonlinear) oscillator systems [43], showing numerically and by using a fractional-nonlinear-diffusion approach that energy transport is subdiffusive. This helps further motivate the study of modulated systems, such as the AA model, in granular chains. In our case, the equations of motion are

$$\ddot{u}_n = [\delta + u_{n-1} - u_n]_+^{3/2} - [\delta + u_n - u_{n+1}]_+^{3/2} - \bar{\beta}[1 + \cos(2\pi n\xi)]u_n, \tag{3.9}$$

where $\bar{\beta} > 0$. In this scenario, the Hookean spring constants are positive for all $n$.

### (ii) Model Ib: $\bar{\gamma} \neq 0$ and $\bar{\alpha}_2 = \bar{\beta} = 0$

We now consider chains that consist of particles that include an internal degree of freedom (DOF) (specifically, as mass-in-mass particles) [38]. Previous studies have focused on the generation [39, 40] of such lattices, their travelling-wave solutions [44,45], and their (bright and dark) breather-like excitations [46,47]. These works illustrate that coherent structures and their dynamics are enriched significantly by the presence of the internal DOF. To give one example, incorporating an internal DOF in the particles can lead to non-local solitary waves with non-vanishing tails (so-called 'nanoptera'), which have been observed experimentally in woodpile granular chains [48]. In our setting, we envision embedding a particle in the interior of each host particle, such that a particle and its interior mass are coupled via a linear restitution mechanism (such as a Hookean spring).
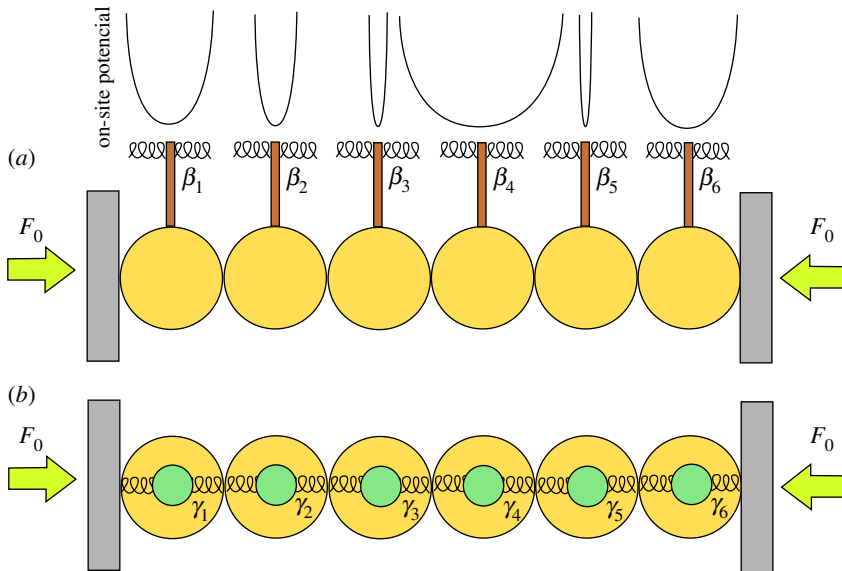
6

rsta.royalsocietypublishing.org  *Phil. Trans. R. Soc. A* **376**: 20170139



**Figure 1.** Schematics of (*a*) model Ia and (*b*) model Ib. Each of these models is a granular chain with an on-site quasiperiodicity. (Online version in colour.)

The equations of motion, upon quasiperiodic modulation of the mass-in-mass (MiM) resonator, are

$$\ddot{u}_n = [\delta + u_{n-1} - u_n]_+^{3/2} - [\delta + u_n - u_{n+1}]_+^{3/2} - \bar{\gamma}[1 + \cos(2\pi n\xi)](u_n - v_n), \qquad (3.10)$$

$$\ddot{v}_n = \bar{\gamma}[1 + \cos(2\pi n\xi)](u_n - v_n), \qquad (3.11)$$

where $\bar{\gamma} > 0$.

## (b) Off-site quasiperiodicity: the Aubry–André model with cylindrical particles

Another approach for incorporating quasiperiodicity in a granular chain is by tuning particle–particle interactions. In existing experimental set-ups, to implement an AA model, one can use chains of cylindrical particles (rather than spherical ones) that are arranged so that their sides are in contact. We are motivated by recent experiments [41] in which it was demonstrated that cylindrical particles offer more flexibility than spherical particles for tuning particle–particle interactions, as one can change the contact angle between contiguous cylinders. Exploiting spatial or even temporal (periodic) variation of contacts between cylindrical particles has been proposed as an efficient way for implementing various functionalities, including that of an acoustic transistor [42].

### (i) Model II: $\bar{\alpha}_2 \neq 0$ and $\bar{\beta} = \bar{\gamma} = 0$

To give equations of motion for a chain of cylindrical particles, we first need to know the form of the Hertzian coefficient in this case. For identical cylinders, the interaction coefficients are [49]

$$\alpha_n(\phi_n) = \frac{Y}{m} g_1(\phi_n) \left[ g_2(\phi_n) \sqrt{g_3(\phi_n)} \right]^{1/2}, \qquad (3.12)$$

where $Y$ depends on the physical parameters of the particles, $m$ is the mass of a particle and $\phi_n$ is the contact angle between cylinders $n - 1$ and $n$ (and is defined mod $\pi/2$). Explicit forms of

$Y$ and $g_i$ are

$$Y = \frac{2E\sqrt{R}}{3(1-\nu^2)},$$

$$g_1(\phi_n) = \sqrt{\frac{1}{\sin(\phi_n)}} \left(\frac{2K[e^2(\phi_n)]}{\pi}\right)^{-3/2},$$

$$g_2(\phi_n) = \frac{4}{\pi e^2(\phi)},$$

$$g_3(\phi_n) = \left(\frac{a^2}{b^2} E[e^2(\phi_n)] - K[e^2(\phi_n)]\right) (K[e^2(\phi_n)] - E[e^2(\phi_n)]),$$

where $E$ is the elastic modulus, $\nu$ is the Poisson ratio, $R$ is the radius of the circular cross section of the cylinders and $e = \sqrt{1-(b/a)^2}$ is the eccentricity of the elliptical area of contact between contiguous cylinders, where $a$ is the semi-major axis length and $b$ is the semi-minor axis length. One can approximate the quotient $b/a$ by $[(1-\cos\phi_n)/(1+\cos\phi_n)]^{2/3}$. The functions $K$ and $E$, respectively, are the complete elliptic integrals of the first and second kinds [50]:

$$K(k) = \int_0^{\pi/2} \frac{d\theta}{\sqrt{1-k^2\sin^2\theta}},$$

$$E(k) = \int_0^{\pi/2} \sqrt{1-k^2\sin^2\theta}\, d\theta,$$

where $k$ is the elliptic modulus.

This yields the following equations of motion:

$$\ddot{u}_n = \alpha_n(\phi_n)[\delta_n + u_{n-1} - u_n]_+^{3/2} - \alpha_{n+1}(\phi_{n+1})[\delta_{n+1} + u_n - u_{n+1}]_+^{3/2}. \tag{3.13}$$

One can control the interactions between particles by changing $\phi_n$ [42]. This raises the following question: What distribution of contact angles $\{\phi_n\}$ yields $\alpha_n(\phi_n) = \bar{\alpha}_1 + \bar{\alpha}_2\cos(2\pi\xi n)$? We address this issue by numerically inverting equation (3.12), so that quasiperiodic variation of $\alpha_n$ yields a quasiperiodic variation of angles in the interval $(\phi_{\min}, \phi_{\max})$. In figure 2, we show the contact-angle distributions for two cases: (i) $\bar{\alpha}_1 = 3$ and $\bar{\alpha}_2 = 1$; and (ii) $\bar{\alpha}_1 = 3$ and $\bar{\alpha}_2 = 3$. We also note that $\alpha(\phi_n) \to \infty$ as $\phi_n \to 0$ and that $\alpha_n(\phi_n)$ has a lower bound at $\phi_n = \pi/2$.

## 4. Linear approximation

Depending on the strength of the precompression that we apply to a granular chain and the magnitude of the strains that arise in (or are exerted on) the chain, one can expand the Hertzian force in a power series about the equilibrium state. This process reduces the equations of motion for the granular chain to ones that resemble those for a Fermi–Pasta–Ulam–Tsingou (FPUT) chain [21]. In particular, if the precompression is strong enough (specifically, if $\delta_n \gg |u_{n-1} - u_n|$ for all $n$), the dominant terms are the linear ones, so we linearize equation (3.11) to get

$$\ddot{u}_n = B_n u_{n-1} + B_{n+1} u_{n+1} - (B_n + B_{n+1} + \beta_n + \gamma_n)u_n + \gamma_n v_n,$$

$$\ddot{v}_n = \gamma_n(u_n - v_n), \tag{4.1}$$

where

$$B_n = \tfrac{3}{2}\alpha_n\delta_n^{1/2}. \tag{4.2}$$

We consider (without loss of generality, at the level of this linear approximation) a complex representation of the wave functions, $u_n = \varphi_n\, e^{i\omega t}$ and $v_n = \psi_n\, e^{i\omega t}$, and we define the notation
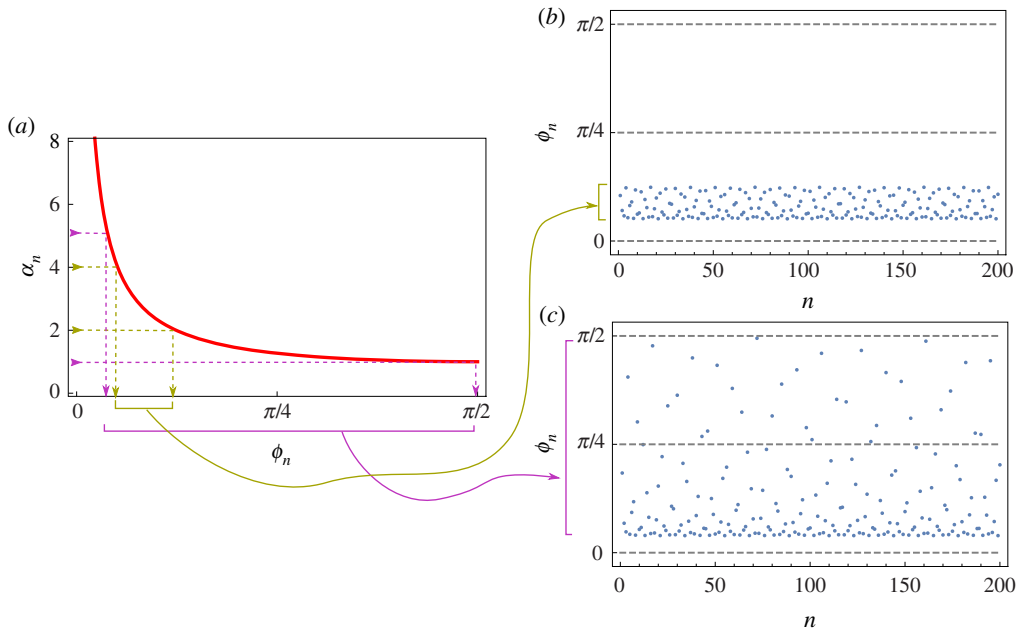
**Figure 2.** (a) Interaction coefficient $\alpha_n$ for model II as a function of the contact angle $\phi_n$ between adjacent cylinders. (b,c) The contact-angle distributions for two cases: (i) $\bar\alpha_1 = 3$ and $\bar\alpha_2 = 1$; and (ii) $\bar\alpha_1 = 3$ and $\bar\alpha_2 = 3$. We use arrows to represent the mapping process that we describe in the text. (Online version in colour.)

$E = -\omega^2$. We thereby obtain the eigenvalue problem

$$E\varphi_n = B_n\varphi_{n-1} + B_{n+1}\varphi_{n+1} - (B_n + B_{n+1} + \beta_n + \gamma_n)\varphi_n + \gamma_n\psi_n,$$

$$E\psi_n = \gamma_n(\varphi_n - \psi_n), \tag{4.3}$$

which we can solve numerically by diagonalization. Using this linear description, we can now address the issue of a localization (metal–insulator) transition for various types of incommensurate periodic coefficients.

## (a) Linear spectrum and localization transition

In addition to the linear spectrum, which we obtain by solving (4.3), we also compute the inverse participation ratio (IPR)

$$P^{-1} = \frac{\sum_n[h(u_n, \dot u_n)^2 + h(v_n, \dot v_n)^2]}{[\sum_n h(u_n, \dot u_n) + h(v_n, \dot v_n)]^2} \in [0, 1] \tag{4.4}$$

as a measure of the amount of localization of the eigenmodes. For modal analysis, we use $h(w, \dot w) = w^2$, where $w \in \{u_n, v_n\}$. (Therefore, $h(u_n, \dot u_n) = u_n^2$ and $h(v_n, \dot v_n) = v_n^2$.) A value of $P^{-1} = 1$ accounts for modes when only one particle is vibrating. By contrast, a mode is fully extended if $P^{-1} \to 0$ as $N \to \infty$, where $N$ is the number of particles in the chain. This provides a qualitative understanding of the nature of the linear modes, and a transition in the IPR also gives a way to quantitatively describe the AA transition.

In figure 3, we show the linear spectrum and IPR as a function of the quasiperiodicity parameter (which is $\bar\beta$ in model Ia and $\bar\gamma$ in model Ib) for a chain of $N = 200$ particles for models Ia and Ib. We observe that these two models have a complex structure of bands and gaps, with some frequencies that appear isolated in the gaps and others that form bands that appear to cluster. Isolated frequencies are associated with modes that are similar to impurity modes. Similar structures of bands and gaps have been observed in other physical systems, such
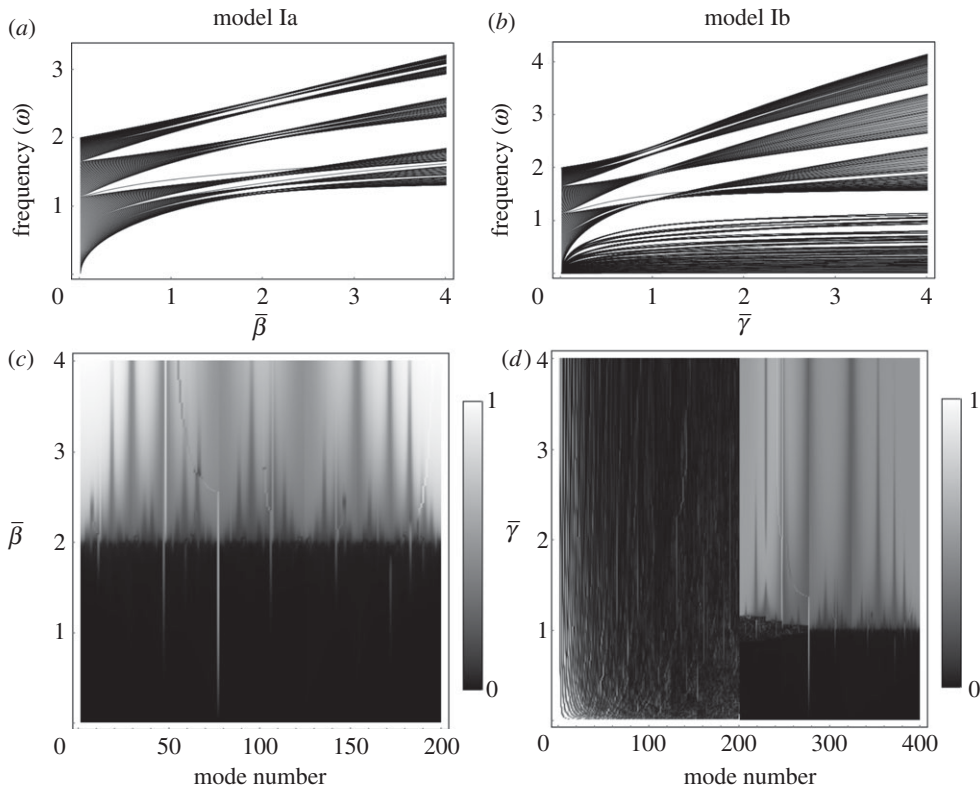
**Figure 3.** (a,b) Linear spectrum of models Ia and Ib as a function of the quasiperiodicity parameter and (c,d) inverse participation ratio (IPR) as a function of mode number and the quasiperiodicity parameter for the two models. We show our results for model Ia in panels (a,c) and for model Ib in panels (b,d).

as in optics (see e.g. [10,32]). Interestingly, we observe from the IPR that AA transitions occur in granular chains, most prominently in model Ia, where the transition is effectively identical to that in the original AA model. This is a consequence of modulating only the on-site potential with an external mechanism, so linearizations of the two systems yield the same equations. If $B_n = 1$ and $\gamma_n = 0$ for all $n$, the transition occurs at $\bar{\beta} = 2$. This differs starkly from the localization properties of the linear modes in the Anderson model, where low-frequency linear modes remain extended independently of the amount of disorder [22]. In figure 4a, we show the transition to localization in the fundamental mode of model Ia. For model Ib, we double the number of modes in the system, because we double the number of DOFs by incorporating the internal particles. This system has a very rich spectrum, where the upper part (constituting half of the modes) has the same structure as in model Ia, but there is also a bottom part (the other half of the modes) associated with modes that do not undergo the localization transition and consequently are extended independently of the modulation. This is straightforward to explain by writing the system (4.1) in terms of in-phase ($x_n = u_n + v_n$) and out-of-phase ($y_n = u_n - v_n$) variables. This yields $\dot{x}_n = f(x_n, x_{n\pm1}, y_n, y_{n\pm1})$ and $\dot{y}_n = g(x_n, x_{n\pm1}, y_n, y_{n\pm1}) - 2\gamma_n y_n$. Only the equations for $\dot{y}_n$ are affected explicitly by the quasiperiodicity. In this case, $2\gamma_n$ enters as a prefactor of $y_n$. This is reminiscent of the prefactor $\beta_n$ from model Ia; and it also explains why the localization transition occurs at $\bar{\gamma} = 1$, instead of at $\bar{\gamma} = 2$. Modes in the upper part of the spectrum also correspond to out-of-phase modes (between $u_n$ and $v_n$), whereas the bottom part of the spectrum is associated with in-phase modes. The latter do not see the quasiperiodicity in practice (because they effectively satisfy the original Hertzian dynamics without the MiM contribution), so they are generically extended.
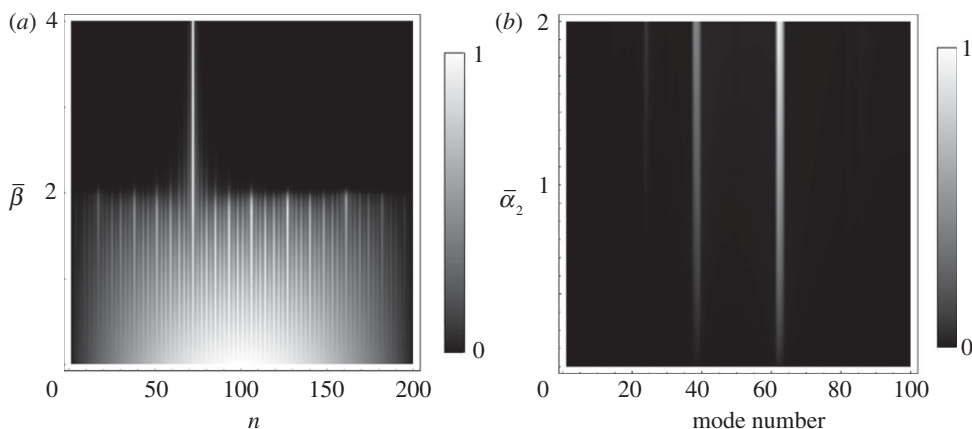
**Figure 4.** (*a*) Localization transition, as evidenced by the absolute value of the amplitude $u_n$ for each $n$, as a function of $\bar{\beta}$ for the fundamental mode in model Ia with $N = 200$ particles. (*b*) Inverse participation ratio as a function of $\bar{\alpha}_2 \in [0, 2]$ (and with $\bar{\alpha}_1 = 3$) for model II with $N = 100$ cylindrical particles.

In contrast with models Ia and Ib, model II (which we recall has an off-site quasiperiodicity) does not have a localization transition. Instead, in model II, we observe that all modes are extended, except for the ones that are associated with isolated frequencies in the gaps. In figure 4*b*, we show the IPR as a function of $\bar{\alpha}_2$ for model II with $\bar{\alpha}_1 = 3$. This suggests that, without an on-site potential, one cannot observe this sort of transition in granular chains of cylindrical particles. In the future, it will be particularly worthwhile to explore the generality of this conclusion. Specifically, a relevant question is whether it is generically the case that it is impossible for inter-site interactions, modulated by one or more frequencies, to induce a localization transition in a granular chain.

## 5. Hofstadter butterfly

Another property of the AA model's spectrum is its fractal nature. To explore this, we compute the spectrum as a function of the parameter $\xi$ (see figure 5), and we observe a structure that is known as a *Hofstadter butterfly*. The butterfly is a footprint of the spectrum's fractality, and one can see its statistical self-similarity in the figure.

The Hofstadter butterfly was first predicted in 1976 [51] in a completely different system: Bloch electrons in 2D lattices and in the presence of orthogonal magnetic fields. In typical crystals, one needs to use magnetic fields that are at least of the order of several thousands of teslas to observe a Hofstadter butterfly. As a result, it took until 1997—in a microwave system [52]—before a Hofstadter butterfly was observed experimentally. A Hofstadter butterfly was then observed in graphene in 2013 [53] and using interacting photons in superconducting qubits in 2017 [54]. The possibility to also observe Hofstadter butterflies in granular chains is very exciting, given the simplicity and controllability of such systems.

### (a) Minkowski–Bouligand fractal dimension of our Hofstadter butterflies

To characterize the self-similarity of the spectrum in the different cases, we compute the Minkowski–Bouligand (MB) fractal dimension ($D_M$), which (by Moran's theorem) is the same as the Hausdorff dimension ($D_H$) for strictly self-similar fractals [55,56]. The procedure that we use to numerically compute $D_M$ is known as 'box counting'. We determine the MB fractal dimension of our butterflies as follows. First, we map the Hofstadter spectrum into a square of $480 \times 480$ pixels; we then partition the square into boxes of characteristic size (side length) $l_B$; and finally
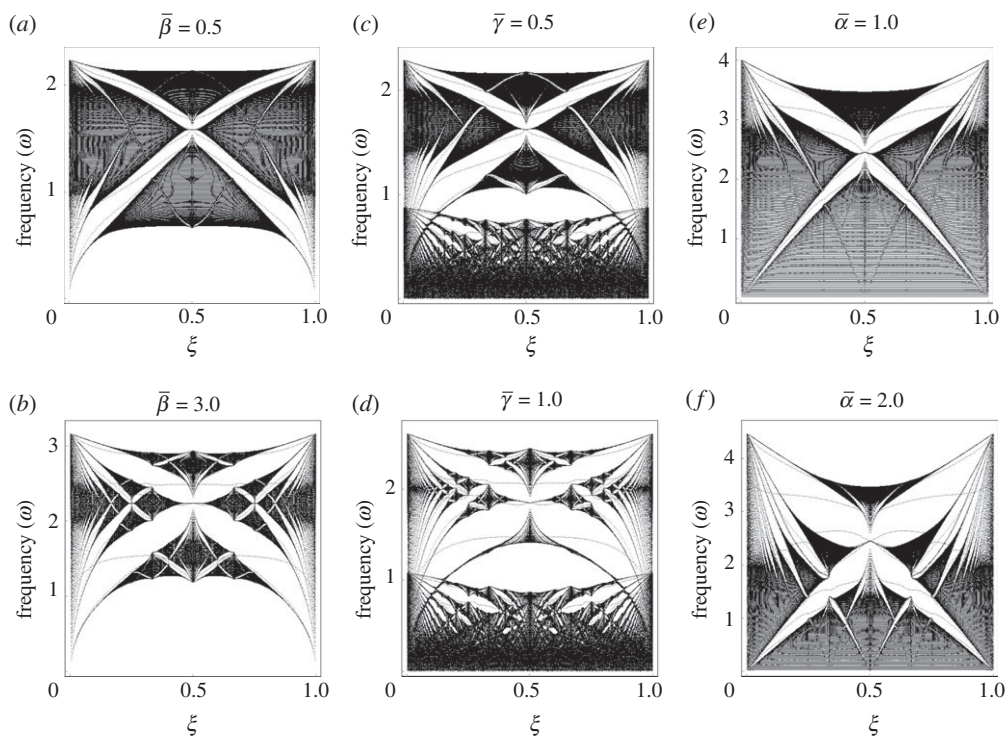
**Figure 5.** Linear spectrum, in the form of a Hofstadter butterfly, as a function of the parameter $\xi$ for (a,b) model Ia, (c,d) model Ib and (e,f) model II.

we count the number $N_B$ of boxes that include at least one point of the spectrum. We do this procedure for different values of $l_B$. If $\ln(N_B)$ scales linearly with $\ln(l_B)$, then the fractal dimension $D_M$ satisfies the relation $N_B \propto l_B^{-D_M}$. In practice, one computes $D_M$ as the best fit to $N_B \propto l_B^{-D_M}$. To do the fitting, we compute a linear regression of the logarithm of the data using gradient descent. In figure 6a, we show an example of the box-counting procedure for the Hofstadter spectrum of model Ia at the localization transition (i.e. when $\bar{\beta} = 2$). To show how the band gaps are filled with boxes, we have superimposed the $N_B$ boxes over the spectrum for different values of $l_B$.

We now compute the fractal dimension $D_M$ as a function of the quasiperiodicity parameters $\bar{\alpha}_2$, $\bar{\beta}$ and $\bar{\gamma}$ for our three models. We expect $D_M$ to be between 1 and 2, because $D_M = 1$ for a line and $D_M = 2$ for a plane. In figure 6b, we show the results of our computations. We observe that the minimum fractal dimension occurs at the same point as the localization transition for models Ia (at $\bar{\beta} = 2$) and Ib (at $\bar{\gamma} = 1$). We calculate that $D_M \gtrsim 1.69$ for model Ia and $D_M \gtrsim 1.82$ for model Ib. It is interesting to note the similar non-monotonic dependence of the fractal dimension on the model parameters in models Ia and Ib. Presumably, this arises from the aforementioned similarity between the former model and the out-of-phase excitations of the latter model. By contrast, in model II, for $\bar{\alpha}_1 = 3$ and $\bar{\alpha}_2 \in (0, 3)$, we observe that the fractal dimension decreases monotonically as $\bar{\alpha}_2$ increases.

## (b) Recovering a Hofstadter butterfly from dynamics

We are interested in reconstructing the Hofstadter spectrum from the dynamics of each of our systems. We are inspired by recent results in interacting photons by Roushan *et al.* [54], who used a technique based on a spectroscopic method and a Fourier transform to resolve the energy levels of a (few-DOF) Bose–Hubbard system. In our case, rather than focusing on resolving each energy level—which one can do in principle by following the procedure from [54]—we visualize the main band-gap structure of a Hofstadter spectrum. To do this, we apply a periodic driving at one
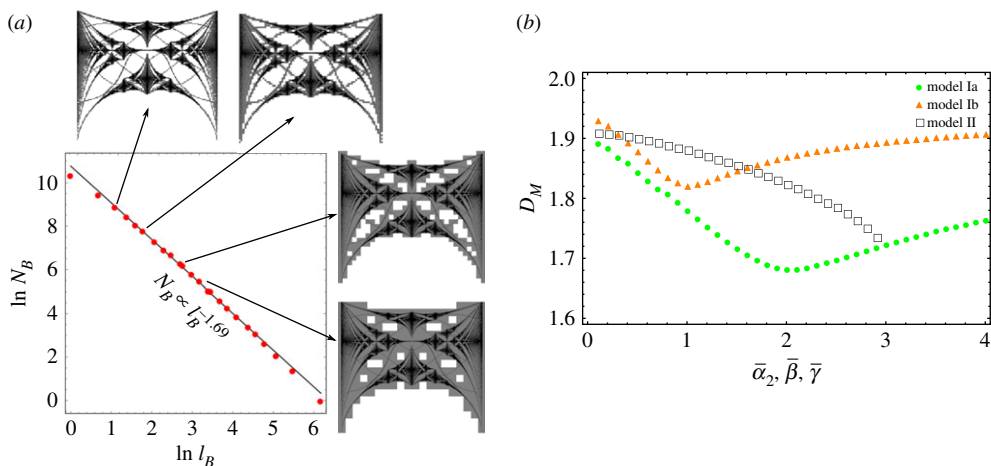
**Figure 6.** (a) Example of the box-counting process that we use to compute the fractal dimension for model Ia (with $\bar{\beta} = 2$). (b) Minkowski–Bouligand fractal dimension $D_M$ as a function of the quasiperiodicity parameter $\bar{\beta}$, $\bar{\gamma}$ and $\bar{\alpha}_2$ for models Ia, Ib and II, respectively. We use the parameter value $\bar{\alpha}_1 = 3$ in model II. (Online version in colour.)

of the boundaries of a granular chain at rest and at various frequencies between the upper and lower band edges. We then measure the energy that is absorbed by the chain after a certain time due to resonances between the excited frequencies and the chain's eigenmodes.

To illustrate our approach, we apply it to model II for a chain with $N = 21$ particles. The external driving is reflected in the first particle's equation of motion:

$$\ddot{u}_1 = \alpha_1 [\delta_1 + \epsilon \sin(2\pi \nu t) - u_1]_+^{3/2} - \alpha_2 [\delta_2 + u_1 - u_2]_+^{3/2}, \tag{5.1}$$

where we use the static precompressive force $F_0 = 100$ and $\epsilon = 0.01$ in our numerical computations. We also set $u_{N+1} = 0$ for all $t$ in equation (3.1), so we have a fixed boundary condition at the other end.

We need to compute the total energy of the system. To do this, we write the $n$th particle's energy as

$$H_n = \frac{\dot{u}_n^2}{2} + \frac{\dot{v}_n^2}{2} + \frac{1}{2} \left\{ \frac{2\alpha_n}{5} [\delta_n + u_{n-1} - u_n]_+^{5/2} + \frac{2\alpha_{n+1}}{5} [\delta_{n+1} + u_n - u_{n+1}]_+^{5/2} \right\}$$

$$+ \frac{\beta_n}{2} u_n^2 + \frac{\gamma_n}{2} (u_n - v_n)^2, \quad n \in \{2, \dots, N\}. \tag{5.2}$$

The energy $H_1$ has the same form as the energy for particles $2, \dots, N$, except for a contribution from the boundary (such as an oscillatory-in-time term when we drive the system).

The total energy is $H = \sum_n H_n$, which is a conserved quantity in the absence of external driving. In the context of experiments, one should also consider dissipation, which we neglect. (See the discussion in [21].) Importantly, we expect that our results will be robust enough to be observable experimentally even in the presence of a small amount of dissipation. This assertion is supported by recent experimental results on the observation of other linear phenomena (e.g. Anderson-like localization [24] and an analogue of a Ramsauer–Townsend resonance [25]) in granular chains.

The system starts at rest at $t = 0$, so $H(0) = \sum_n (2\alpha_n/5)\delta_n^{5/2}$ is the constant background energy associated with the precompression. Moreover, for $t > 0$, we have $H(t) \geq H(0)$ in the presence of the drive. Let $\Delta H(T) = H(T) - H(0) \geq 0$ denote the energy that is absorbed by the system at time $t = T$. To integrate equations (3.1) and (5.1), along with equation (3.2), we use a fifth-order explicit Runge–Kutta (RK5) method with a step size of $dt = 0.01$ and time $T = 20$. In figure 7, we show the absorbed energy patterns for two sets of parameters: (i) $\bar{\alpha}_1 = 3$ and $\bar{\alpha}_2 = 1$; and (ii) $\bar{\alpha}_1 = 3$ and
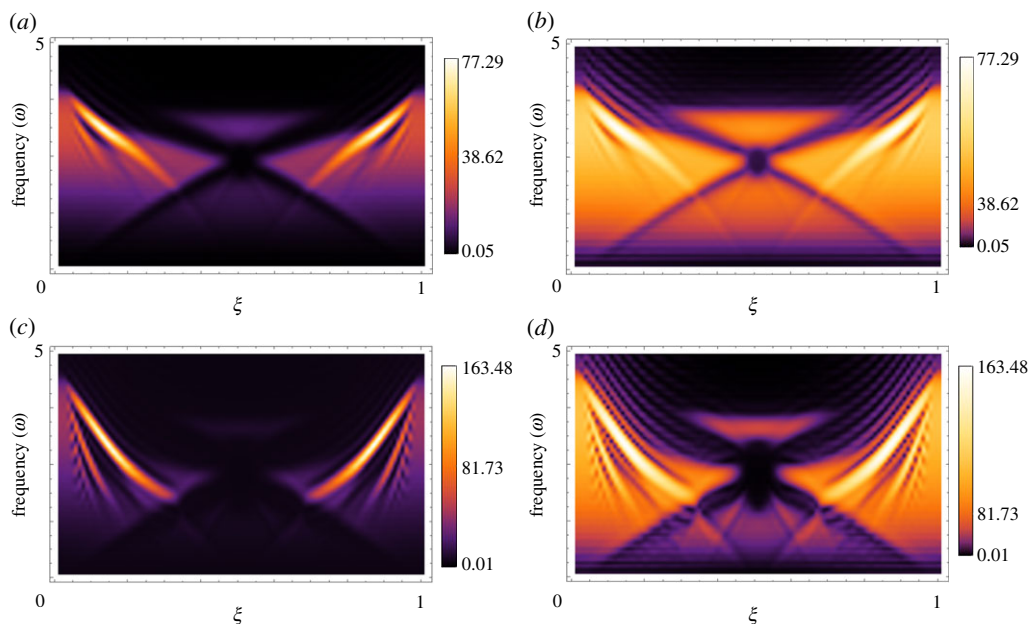
**Figure 7.** Energy absorbed in model II for $(a,b)$ $\bar{\alpha}_2 = 1$ and $(c,d)$ $\bar{\alpha}_2 = 2$. We use the parameter value $\bar{\alpha}_1 = 3$ in all cases. We show the absorbed energy on a linear scale in $(a,c)$ and on a logarithmic scale in $(b,d)$. High intensity corresponds to a large absorbed energy and hence to frequencies in the passband of the system, whereas a low intensity corresponds to frequencies in the band gaps of the system. (Online version in colour.)

$\bar{\alpha}_2 = 2$. By comparing these patterns with figure 5, we see that our method is very effective at capturing the main band-gap structure, and we are even able to successfully capture some fine structure (i.e. some minor gaps), which we can observe especially when we plot the logarithm of the absorbed energy.

## 6. Energy transport and localization

Another important issue, which one can examine in several ways, is how energy transport is affected by the quasiperiodicity [57,58]. For instance, one can compute a second moment $m_2$ of the energy distribution as a function of time to quantitatively characterize the temporal evolution of the energy distribution's width [22–24,59–64]. Following recent studies in disordered granular chains [24], we study the evolution of the energy distribution $\{H_n\}_{n=1}^{N}$ immediately after the impact of a striker against the first particle ($n = 1$). In the context of experiments, one should also consider dissipation, which we neglect. (Again, see [21] for a discussion.) Importantly, we expect that our results will be robust enough to be observable experimentally even in the presence of a small amount of dissipation. This assertion is supported by recent experimental results on other linear phenomena in granular chains [24,25].

We compute the second moment

$$m_2(t) = \frac{\sum_n (n-1)^2 H_n}{\sum_n H_n}, \tag{6.1}$$

and we estimate a scaling relationship between $m_2$ and $t$. When the scaling is approximated reasonably as a power law (for which, in exact form, $m_2(t) \sim t^\eta$ as $t \to \infty$ for some exponent $\eta$), one can categorize cases with $\eta = 2$ as *ballistic*, cases with $\eta \in (1,2)$ as *superdiffusive*, cases with $\eta = 1$ as *diffusive*, and cases with $\eta \in (0,1)$ as *subdiffusive*. If $\eta = 0$, we say that there is no diffusion; in other words, all energy remains localized. In a perfectly homogeneous granular chain, it is
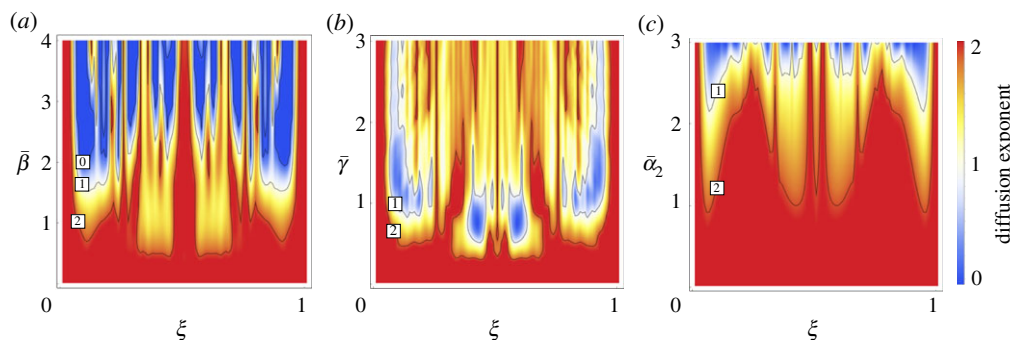
**Figure 8.** Diffusion exponent $\eta$ for (*a*) model Ia, (*b*) model Ib and (*c*) model II as a function of the quasiperiodicity parameters and $\xi$. The boxed numbers label curves of transition between different energy-transport regimes: '2' for the transition between superdiffusive and ballistic transport, '1' for diffusive transport (because the exponent is 1 on that curve), and '0' (in model 1a only) for a localization transition. (Online version in colour.)

known that energy transport is ballistic. However, for a chain with disorder, the dynamics can be markedly different, and there exist different energy-transport regimes [22–24]. These previous studies focused on the interplay between disorder and nonlinearity. Here, by contrast, we show that, even in a strongly precompressed (i.e. almost linear) chain, one can obtain any desired diffusion exponent $\eta \in [0, 2]$ for the energy transport. However, we find that on-site potentials are essential to have localization.

One advantage of working with quasiperiodic chains instead of disordered ones is that we do not need to compute averages over a large number of realizations to obtain robust insights. We construct our quasiperiodic chains in a deterministic way, so, given a parameter $\xi$, there is one specific chain. This enables us to cover the whole parameter space with considerably fewer computations than when studying disordered chains. We are also interested in characterizing energy transport in realistic frameworks, so we set the number of particles to be $N = 21$, which gives a long enough chain to qualitatively capture the nature of transport, at least in several recent experimental and theoretical explorations [22,24].

As in §5b, we integrate equations (3.1,3.2) using an RK5 method. Additionally, we set $u_0(t) = u_{N+1}(t) = 0$ for all $t$, so we have fixed boundary conditions on both sides. In our simulations, our stopping criteria are that either $T = 20$ or energy reaches the boundary opposite to the one that is impacted by a striker. We use the former condition to stop the code in cases in which all of the energy is trapped in the form of localized states. In other words, there is no diffusion. This is expected, for instance, in model Ia for $\bar{\beta} > 2$ (i.e. after the localization transition occurs). However, it is an uncommon scenario in model II, which does not have a localization transition. In figure 8, we show our results for energy transport in our three models. In models Ia and Ib, we explore the parameter ranges $\bar{\beta} \in [0, 4]$ and $\bar{\gamma} \in [0, 3]$, respectively, so we can compare energy transport on both sides of the localization transition. In model II, we consider $\bar{\alpha}_1 = 3$ and $\bar{\alpha}_2 \in [0, 3]$. For all three models, and with $\xi \in [0, 1]$, we can tune the energy transport from subdiffusive to ballistic behaviours. This allows a great deal of control of the energy-transport properties, and it is remarkable that we are able to do this using a deterministic model. In model Ia, we also observe localization (for which $\eta = 0$), in contrast with observations in disordered granular chains [22–24]. This suggests that the inclusion of on-site potentials is crucial for this localization phenomenon.

## 7. Conclusions and discussion

We introduced different types of quasiperiodic granular chains that are inspired by the work of Aubry and André in condensed-matter physics and by recent developments (cradle and mass-in-mass systems) in granular lattice systems. We studied the localization and spectral properties of such chains. To construct each type of quasiperiodic chain, we incorporated spatial modulation

15

rsta.royalsocietypublishing.org   *Phil. Trans. R. Soc. A* **376**: 20170139

(in a form that is incommensurate with the chain's period) into one of the physical parameters. We proposed three models: models Ia and Ib use spherical particles, and quasiperiodicity enters via an on-site potential, in the form of either a local oscillator (as in a cradle) or a local resonator (for a mass-in-mass system); and model II uses cylindrical particles and has off-site quasiperiodicity. In models Ia and Ib, we demonstrated the existence of an analogue of the well-known AA transition. However, in model II, we showed that, without an on-site potential and with quasiperiodicity affecting only inter-site interactions, a localization transition cannot occur.

We also computed the Hofstadter spectrum for each of the models and studied their fractal properties by computing the Minkowski–Bouligand fractal dimension. In models Ia and Ib, we showed that the minimum fractal dimension $D_M$ of the spectrum coincides with the point at which the localization transition occurs. For model II, we observed that the spectrum's fractal dimension decreases monotonically as a function of the quasiperiodicity parameter, and we showed how to construct the Hofstadter spectrum from the system dynamics.

Finally, we numerically studied energy transport by exciting the granular chains with a striker. We demonstrated the existence of different regimes—ranging from ballistic to subdiffusive transport—as well as localization. In contrast with prior work, which achieved such control using a combination of disorder and adjustment of the nonlinearity strength [22–24], we were able to control the energy transport using a deterministic model in a strongly precompressed (and almost linear) granular chain.

Naturally, it will be particularly valuable to implement some of these ideas in laboratory experiments, as one can then further explore the role that granular systems can play in the study of systems with quasiperiodicity [52–54]. Achieving an experimental realization of a Hofstadter butterfly in a granular chain would also be very exciting in its own right. Among the settings that we have proposed in this paper, model Ib (i.e. the chain of mass-in-mass particles) is the clearest candidate for observing a localization transition (in the out-of-phase variables), given that the cradle system has yet to be realized experimentally. Arguably, the woodpile set-up of [48] may also constitute an excellent playground for such studies. However, a key consideration, given experimental limitations, is that it is desirable to build a chain with as few particles as possible such that one can (still) observe the relevant phenomenology.

There are also numerous open issues to explore computationally and theoretically. Examples include the effect of nonlinearity (e.g. through larger excitation amplitudes) on these modes and their localization, how these phenomena differ for granular crystals in different numbers of dimensions, and others.

# References

1. Janot C. 1994 *Quasicrystals: a primer*, 2nd edn. Oxford, UK: Clarendon Press.
2. Bindi L, Steinhardt PJ, Yao N, Lu PJ. 2009 Natural quasicrystals. *Science* **324**, 1306–1309. (doi:10.1126/science.1170827)
3. Lifshitz R. 2003 Quasicrystals: a matter of definition. *Found. Phys.* **33**, 1703–1711. (doi:1023/A: 1026247120031)
4. Penrose R. 1978 Pentaplexity. *Eureka* **39**, 16–32.
5. Levine D, Steinhardt PJ. 1984 Quasicrystals: a new class of ordered structures. *Phys. Rev. Lett.* **53**, 2477. (doi:10.1103/PhysRevLett.53.2477)
6. Aubry S, André G. 1980 Analyticity breaking and Anderson localization in incommensurate lattices. *Ann. Isr. Phys. Soc.* **3**, 133–164.

16

rsta.royalsocietypublishing.org  *Phil. Trans. R. Soc. A* **376**: 20170139

7. Kraus YE, Zilberberg O. 2012 Topological equivalence between the Fibonacci quasicrystal and the Harper model. *Phys. Rev. Lett.* **109**, 116404. (doi:10.1103/PhysRevLett.109.116404)

8. Grempel DR, Fishman S, Prange RE. 1982 Localization in an incommensurate potential: an exactly solvable model. *Phys. Rev. Lett.* **49**, 833. (doi:10.1103/PhysRevLett.49.833)

9. Aullbach C, Wobst A, Ingold G-L, Hänggi P, Varga I. 2004 Phase-space visualization of a metal–insulator transition. *New J. Phys.* **6**, 70. (doi:10.1088/1367-2630/6/1/070)

10. Lahini Y, Pugatch R, Pozzi F, Sorel M, Morandotti R, Davidson N, Silberberg Y. 2009 Observation of a localization transition in quasiperiodic photonic lattices. *Phys. Rev. Lett.* **103**, 013901. (doi:10.1103/PhysRevLett.103.013901)

11. Flach S, Ivanchenko M, Khomeriki R. 2012 Correlated metallic two-particle bound states in quasiperiodic chains. *Europhys. Lett.* **98**, 66002. (doi:10.1209/0295-5075/98/66002)

12. Iyer S, Oganesyan V, Refael G, Huse DA. 2013 Many-body localization in a quasiperiodic system. *Phys. Rev. B* **87**, 134202. (doi:10.1103/PhysRevB.87.134202)

13. Mastropietro V. 2015 Localization of interacting fermions in the Aubry–André model. *Phys. Rev. Lett.* **115**, 180401. (doi:10.1103/PhysRevLett.115.180401)

14. Bordia D, Lüschen H, Schneider U, Knap M, Bloch I. 2017 Periodically driving a many-body localized quantum system. *Nat. Phys.* **13**, 460–464. (doi:10.1038/nphys4020)

15. Romito D, Lobo C, Recati A. 2018 Localisation transition in the driven Aubry–André model. (http://arxiv.org/abs/1802.08859)

16. Smith A, Knolle J, Kovrizhin DL, Roessner R. 2017 Disorder-free localization. *Phys. Rev. Lett.* **118**, 266601. (doi:10.1103/PhysRevLett.118.266601)

17. Devakul T, Huse DA. 2017 Anderson localization transitions with and without random potentials. *Phys. Rev. B* **96**, 214201. (doi:10.1103/PhysRevB.96.214201)

18. Nesterenko VF. 2001 *Dynamics of heterogeneous materials*. Heidelberg, Germany: Springer.

19. Sen S, Bang J, Avalos E, Doney R. 2008 Solitary waves in the granular chain. *Phys. Rep.* **462**, 21–66. (doi:10.1016/j.physrep.2007.10.007)

20. Porter MA, Kevrekidis PG, Daraio C. 2015 Granular crystals: nonlinear dynamics meets materials engineering. *Phys. Today* **68**(11), 44. (doi:10.1063/PT.3.2981)

21. Chong C, Porter MA, Kevrekidis PG, Daraio C. 2017 Nonlinear coherent structures in granular crystals. *J. Phys.: Condens. Matter* **29**, 413003. (doi:10.1088/1361-648X/aa7672)

22. Martínez AJ, Kevrekidis PG, Porter MA. 2016 Superdiffusive transport and energy localization in disordered granular crystals. *Phys. Rev. E* **93**, 022902. (doi:10.1103/PhysRevE.93.022902)

23. Achilleos V, Theocharis G, Skokos C. 2016 Energy transport in one-dimensional disordered granular solids. *Phys. Rev. E* **93**, 022903. (doi:10.1103/PhysRevE.93.022903)

24. Kim E, Martínez AJ, Phenisee SE, Kevrekidis PG, Porter MA, Yang J. 2018 Direct measurement of superdiffusive energy transport in disordered granular chains. *Nat. Commun.* **9**, 640. (doi:10.1038/s41467-018-03015-3)

25. Martínez AJ, Yasuda H, Kim E, Kevrekidis PG, Porter MA, Yang J. 2016 Scattering of waves by impurities in precompressed granular chains. *Phys. Rev. E* **93**, 052224. (doi:10.1103/PhysRevE.93.052224)

26. Boechler N, Theocharis G, Daraio C. 2011 Bifurcation-based acoustic switching and rectification. *Nat. Mater.* **10**, 665–668. (doi:10.1038/nmat3072)

27. Starosvetsky Y, Jayaprakash KR, Arif Hasan M, Vakakis AF. 2017 *Topics on the nonlinear dynamics and acoustics of ordered granular media*. Singapore: World Scientific.

28. Lindenberg K, Harbola U, Romero AH, Lindenberg K. 2011 Pulse propagation in granular chains. *AIP Conf. Proc.* **1339**, 97. (doi:10.1063/1.3574848)

29. Przedborski M, Sen S, Harroun TA. 2017 Fluctuations in Hertz chains at equilibrium. *Phys. Rev. E* **95**, 032903. (doi:10.1103/PhysRevE.95.032903)

30. Han D, Westley M, Sen S. 2014 Mechanical energy fluctuations in granular chains: the possibility of rogue fluctuations or waves. *Phys. Rev. E* **90**, 032904. (doi:10.1103/PhysRevE.90.032904)

31. Anderson PW. 1958 Absence of diffusion in certain random lattices. *Phys. Rev.* **109**, 1492. (doi:10.1103/PhysRev.109.1492)

32. Martínez AJ, Molina MI. 2012 Surface solitons in quasiperiodic nonlinear photonic lattices. *Phys. Rev. A* **85**, 013807. (doi:10.1103/PhysRevA.85.013807)

33. Roati G, D'Errico C, Fallani L, Fattori M, Fort C, Zaccanti M, Modugno G, Modugno M, Inguscio M. 2008 Anderson localization of a non-interacting Bose–Einstein condensate. *Nature* **453**, 895–898. (doi:10.1038/nature07071)

34. Yuce C. 2014 PT symmetric Aubry–André model. *Phys. Lett. A* **378**, 2024–2028. (doi:10.1016/j.physleta.2014.05.005)

35. Goldstein M, Schlag W, Voda M. 2017 On the spectrum of multi-frequency quasiperiodic Schrödinger operators with large coupling. (http://arxiv.org/abs/1708.09711)

36. James G. 2011 Nonlinear waves in Newton's cradle and the discrete *p*-Schrödinger equation. *Math. Models Methods Appl. Sci.* **21**, 2335. (doi:10.1142/S0218202511005763)

37. James G, Kevrekidis PG, Cuevas J. 2013 Breathers in oscillator chains with Hertzian interactions. *Physica D* **251**, 39–59. (doi:10.1016/j.physd.2013.01.017)

38. Huang H, Sun C, Huang G. 2009 On the negative effective mass density in acoustic metamaterials. *Int. J. Eng. Sci.* **47**, 610–617. (doi:10.1016/j.ijengsci.2008.12.007)

39. Kevrekidis PG, Vainchtein A, Serra Garcia M, Daraio C. 2013 Interaction of traveling waves with mass-with-mass defects within a Hertzian chain. *Phys. Rev. E* **87**, 042911. (doi:10.1103/PhysRevE.87.042911)

40. Bonanomi L, Theocharis G, Daraio C. 2015 Wave propagation in granular chains with local resonances. *Phys. Rev. E* **91**, 033208. (doi:10.1103/PhysRevE.91.033208)

41. Khatri D, Ngo D, Daraio C. 2012 Highly nonlinear solitary waves in chains of cylindrical particles. *Granul. Matter* **14**, 63–69. (doi:10.1007/s10035-011-0297-9)

42. Li F, Chong C, Yang J, Kevrekidis PG, Daraio C. 2014 Wave transmission in time- and space-variant helicoidal phononic crystals. *Phys. Rev. E* **90**, 053201. (doi:10.1103/PhysRevE.90.053201)

43. Mulansky M, Pikovsky A. 2013 Energy spreading in strongly nonlinear disordered lattices. *New J. Phys.* **15**, 053015. (doi:10.1088/1367-2630/15/5/053015)

44. Xu H, Kevrekidis PG, Stefanov A. 2015 Traveling waves and their tails in locally resonant granular systems. *J. Phys. A* **48**, 195204. (doi:10.1088/1751-8113/48/19/195204)

45. Vorotnikov K, Starosvetsky Y, Theocharis G, Kevrekidis PG. 2018 Wave propagation in a strongly nonlinear locally resonant granular crystal. *Physica D* **365**, 27–41. (doi:10.1016/j.physd.2017.10.007)

46. Liu L, James G, Kevrekidis PG, Vainchtein A. 2016 Strongly nonlinear waves in locally resonant granular chains. *Nonlinearity* **29**, 3496. (doi:10.1088/0951-7715/29/11/3496)

47. Liu L, James G, Kevrekidis PG, Vainchtein A. 2016 Breathers in a locally resonant granular chain with precompression. *Physica D* **331**, 27–47. (doi:10.1016/j.physd.2016.05.007)

48. Kim E, Li F, Chong C, Theocharis G, Yang J, Kevrekidis PG. 2015 Highly nonlinear wave propagation in elastic woodpile periodic structures. *Phys. Rev. Lett.* **114**, 118002. (doi:10.1103/PhysRevLett.114.118002)

49. Johnson KL. 1987 *Contact mechanics*. Cambridge, UK: Cambridge University Press.

50. National Institute of Standards and Technology. 2015 Digital Library of Mathematical Functions (release 1.0.10). See http://dlmf.nist.gov/.

51. Hofstadter DR. 1976 Energy levels and wavefunctions of Bloch electrons in rational and irrational magnetic fields. *Phys. Rev. B* **14**, 2239. (doi:10.1103/PhysRevB.14.2239)

52. Kuhl U, Stöckmann H-J. 1998 Microwave realization of the Hofstadter butterfly. *Phys. Rev. Lett.* **80**, 3232. (doi:10.1103/PhysRevLett.80.3232)

53. Dean CR *et al.* 2013 Hofstadter's butterfly and the fractal quantum Hall effect in moiré superlattices. *Nature* **497**, 598–602. (doi:10.1038/nature12186)

54. Roushan P *et al.* 2017 Spectroscopic signature of localization with interacting photons in superconducting qubits. *Science* **358**, 1175–1179. (doi:10.1126/science.aao1401)

55. Falconer K. 2014 *Fractal geometry: mathematical foundations and applications*, 3rd edn. Hoboken, NJ: Wiley-Blackwell.

56. Schroeder M. 1991 *Fractals, chaos, power laws: minutes from an infinite paradise*. New York, NY: W. H. Freeman.

57. Kramer B, MacKinnon A. 1993 Localization: theory and experiment. *Rep. Prog. Phys.* **56**, 1469–1564. (doi:10.1088/0034-4885/56/12/001)

58. Laptyeva TV, Ivanchenko MV, Flach S. 2014 Nonlinear lattice waves in heterogeneous media. *J. Phys. A* **47**, 493001. (doi:10.1088/1751-8113/47/49/493001)

59. Datta PK, Kundu K. 1995 Energy transport in one-dimensional harmonic chains. *Phys. Rev. B* **51**, 6287. (doi:10.1103/PhysRevB.51.6287)

60. Lepri S, Schilling R, Aubry S. 2010 Asymptotic energy profile of a wave packet in disordered chains. *Phys. Rev. E* **82**, 056602. (doi:10.1103/PhysRevE.82.056602)

61. Naether U, Rojas-Rojas S, Martínez AJ, Stützer S, Tünnermann A, Nolte S, Molina MI, Vicencio RA, Szameit A. 2013 Enhanced distribution of a wave-packet in lattices with disorder and nonlinearity. *Opt. Express* **21**, 927. (doi:10.1364/OE.21.000927)

62. García-Mata I, Shepelyansky DL. 2009 Delocalization induced by nonlinearity in systems with disorder. *Phys. Rev. E* **79**, 026205. (doi:10.1103/PhysRevE.79.026205)

63. Laptyeva TV, Bodyfelt JD, Krimer DO, Skokos C, Flach S. 2010 The crossover from strong to weak chaos for nonlinear waves in disordered systems. *Europhys. Lett.* **91**, 30001. (doi:10.1209/0295-5075/91/30001)

64. Rojas-Rojas S, Morales-Inostroza L, Naether U, Xavier GB, Nolte S, Szameit RA, Vicencio R, Lima G, Delgado A. 2014 Analytical model for polarization-dependent light propagation in waveguide arrays and applications. *Phys. Rev. A* **90**, 063823. (doi:10.1103/PhysRevA. 90.063823)